Supporting information

Facile self-propagated carbonization synthesis of phosphorus-doped carbon based catalysts for partial oxidation and hydrogenation

Huan Wang[a], Weitao Wang[a,*], Xulu Jiang[a], Zhen-Hong He[a], Kuan Wang[a], Yang Yang[a], Zhao-Tie Liu[a,b,*] and Buxing Han[c,*]

[a] *College of Chemistry & Chemical Engineering, Shaanxi Key Laboratory of Chemical Additives for Industry, Shaanxi University of Science & Technology, Xi'an, Shaanxi, 710021, China.*

[b] *School of Chemistry & Chemical Engineering, Shaanxi Normal University, Xi'an, Shaanxi, 710119, China.*

[c] *Beijing National Laboratory for Molecular Sciences (BNLMS), Centre for Molecular Science, Institute of Chemistry, Chinese Academy of Sciences, Beijing 100190, China*

**E-mail: wangweitao@sust.edu.cn (Weitao. Wang), ztliu@snnu.edu.cn (Zhao-Tie. Liu), Hanbx@iccas.ac.cn (Buxing. Han)*

Materials

Fructose (99%), glucose (99% biotech grade), cellulose powder (particle size: 25 μm) and chitosan (degree of deacetylation ≥95%, viscosity 100-200 mpa·s) were purchased from Shanghai Macklin Biochemical Co., Ltd. Sucrose (AR) was purchased from Guangzhou Jinhuada Chemical Reagent Co., Ltd. P_2O_5 (>98%), $ZrOCl_2 \cdot 8H_2O$ (>98%), $PdCl_2$ (>98%), and methanol (AR, ≥99.5%) were obtained from Shanghai Titan Technology Co., Ltd. The other reagents used were analytical grade without further purification.

Preparation of phosphorus-doped carbon (PDC) materials

Precautions: The SPC process is an exothermic process and is accompanied by the production of some water vapor and gases from the carbonization of the biomass. The highest temperature in the SPC process was measured to be in the range of 260 to 270 °C. Therefore, the operation of this reaction process requires care to prevent scalding and to be carried out under ventilated conditions.

Characterizations of Catalysts

The X-ray diffraction was carried out on Rigaku D/max 2500 with nickel filtered Cu-Kα (λ=0.154 nm) operated at 40 kV and 20 mA. Scanning electron microscopy charaterization was carried out at 20 kV and 15 mA on the Hitachi S-4800. Fourier transform infrared spectroscopy was performed on a VECTOR-22 using the KBr pellet technique with a resolution of 2 cm^{-1} at room temperature. XPS spectra were obtained from ThermoFisher's ESCALAB 250Xi electronic spectrometer, using a monochromatic Al Kα source (Mono Al Kα) radiation source (1486.6 eV) and a hemispherical energy analyzer. All binding energies were corrected based on the C1s peak (284.8 eV). The Raman spectra were collected on a Laser microscopic Raman imaging spectrometer (Thermo Fisher, USA) equipped with a 532 nm Ne laser and a high-grade Leica microscope (long working distance objective 50). The N_2 adsorption/desorption tests were carried out at -196 °C using a Micromeritics ASAP 2460 (USA). Prior to measurements, the samples were degassed at 200 °C

for 12 h under vacuum (lower than 10^{-5} tor). ICP-OES was detected with an Aglient 5110 instrument (instrument parameters: Pump Rate, 100 r/min; Nebulizer Flow, 28.0 psi; Auxiliary Gas, 0.5 ipm; Sample Flush Time, 20 s; RF Power, 1150w). Py-FTIR spectroscopy adopted tensor 27 Fourier infrared spectrometer produced by Bruker, the in-situ cell is a CaF_2 window, collected 32 times with a resolution of 4 cm^{-1}.

Table S1. Yield of PDC materials.

Entry	Fructose (g)	P_2O_5 (g)	$ZrOCl_2 \cdot 8H_2O$ (g)	$PdCl_2$ (g)	PDC material yield (wt.%)[a]
PDC	2.0	1.6	/	/	69.7
Zr/PDC	2.0	1.6	0.2	/	66.1
Pd/PDC	2.0	1.6	/	0.05	68.2
PdZr/PDC	2.0	1.6	0.2	0.05	64.9
$PdZr/PDC_{(\times 5)}$ [b]	10.0	8.0	1.0	0.25	68.7

[a] The yield of PDC material: (the mass of obtained PDC materials)/(mass of total raw substrates).

[b] The sample preparation was amplified to 5 fold.

Table S2. Content of each element in different catalysts. [a]

Entry	Catalyst	P wt.%	Zr wt.%	Pd wt.%
1	PDC	4.43	/	/
2	Pd/PDC	2.20	/	1.83
3	Zr/PDC	4.23	4.08	/
4	PdZr/PDC	0.52	3.53	2.61
5	PdZr/PDC [b]	0.44	4.09	2.64
6	$PdZr/PDC_{(\times 5)}$	0.58	4.02	2.66
7	Pd/C	/	/	2.71
8	PdZr/C	/	3.94	1.71

[a] Elemental content determined by ICP-OES.

[b] PdZr/PDC sample after one use.

Table S3. Relative element content of different catalysts.[a]

Entry	Catalyst	P mol%	Pd mol%	Zr mol%
1	PDC	5.4	/	/
2	Zr/PDC	1.3	/	1.9
3	Pd/PDC	1.1	1.6	/
4	PdZr/PDC	0.9	1.3	1.5

[a] The relative content of elements was obtained by comparing the peak areas of XPS.

Table S4. Acidity for PDC series materials. [a]

Entry	Catalyst	Brønsted acid (μmol/g)	Lewis acid (μmol/g)	L/B
1	Pd/PDC	4.50	36.16	8.04
2	Zr/PDC	4.34	29.95	6.90
3	PdZr/PDC	2.93	26.37	9.01

[a] The acidity of PDC series materials was obtained by Py-IR spectra.

Table S5. The textural structure of different catalysts.

Entry	Catalyst	Specific surface area [a] (m^2/g)	Total volume [b] (cm^3/g)
1	PDC	18	0.0046
2	Zr/PDC	16	0.0041
3	Pd/PDC	83	0.0281
4	PdZr/PDC	69	0.0246

[a] Specific surface area based on the Brunauer-Emmett-Teller equation. [b] The total pore volume.

Table S6. Performance of palladium-based catalysts reported in the literature for the oxidation of benzyl alcohol for the preparation of benzaldehyde.[a]

Entry	Catalyst	T (℃)	*t* (h)	O_2 (MPa)	Conv. (%)	Sel. (%)	TOF (h^{-1})	Ref.
1	2Pd/NOMC	90	3	Air	72	>99	979	[1]
2	0.2MnOx/Pd/Al_2O_3	120	4	0.1	84.7	90.3	31561	[2]
3	Au-Pd/C(SI)	85	6	H_2O_2	47.2	84.8	525.2	[3]
4	3Pd/20ZnSBA	90	7.5	0.1	95.0	80.0	862	[4]
5	0.5 wt% Au-0.5 wt% Pd/TiO_2	80	4	TBHP	19.1	80.5	318.6	[5]
6	Pd–2C–1N	30	15	0.1	76.0	96.0	0.31	[6]
7	PdZr/PDC	60	3	0.1	96.5	92.5	9.2	This work
8	PdZr/PDC	80	2.5	0.1	>99	93.8	22.1	This work

[a] TOF = Number of benzyl alcohol molecules converted per mol Pd per hour.

Table S7. Performance of Pd-based catalysts for the hydrogenation of phenol to prepare cyclohexanone as reported in the literature.[a]

Entry	Catalyst	T (℃)	*t* (h)	H_2 (MPa)	Conv. (%)	Sel. (%)	TOF (h^{-1})	Ref.
1	ACN_{pd}	100	5	1	100	99.1	29.34	[7]
2	Pd@HMSNs	55	4	0.1	≥99.0	98.3	7.82	[8]
3	Pd/C600	80	0.5	0.1	88.3	96.0	199.2	[9]
4	Pd/CN-O-50	140	0.66	0.5	99.6	97.5	2333	[10]
5	Pd/pol-NH_2	100	2	0.3	>99.5	>99.5	10.0	[11]
6	Pd@mpg-C_3N_4	65	2	0.1	>99	>99	10.0	[12]
7	Pd@hydrophilic-C	100	20	1	>99	95	0.57	[13]
8	Pd/C-$AlCl_3$	50	7	1	>99.9	>99.9	2.86	[14]
9	Pd/MIL-101	25	11	0.1	>99.9	>99.9	1.81	[15]
10	10 wt.% Pd/C $CHKO_2$	100	6	/	>99	>99	8.33	[16]
11	PdZr/PDC	50	6	0.1	99.7	98.2	1.45	This work

[a] TOF = Number of phenol molecules converted per mol Pd per hour.

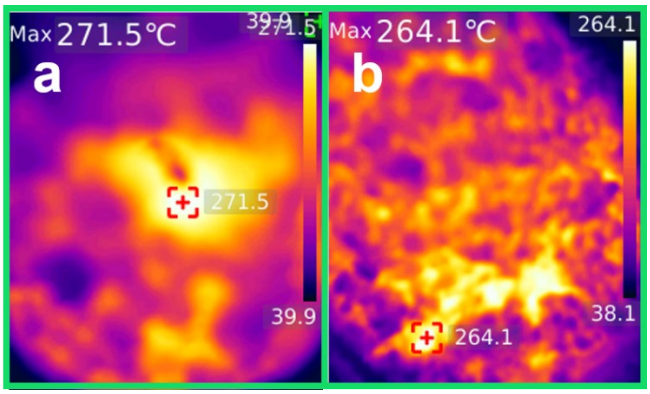

Figure S1. Steady-state temperatures of the SPC reaction as determined by infrared calorimetry. (a) PdZr/PDC; (b) PdZr/PDC$_{(\times 5)}$.

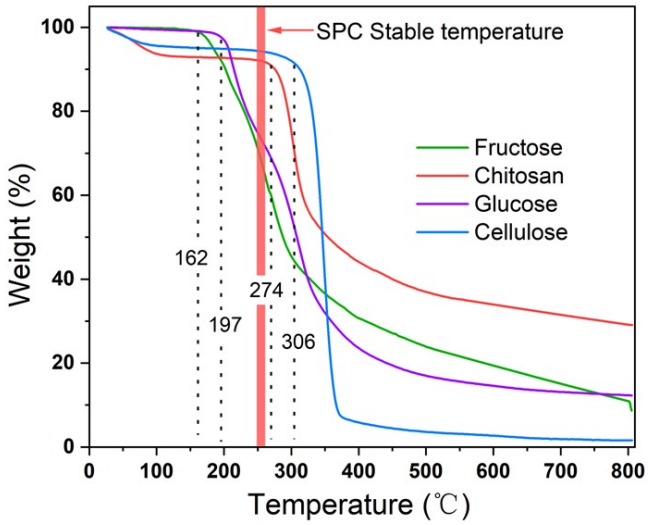

Figure S2. TG analysis of different biomasses.

The thermal stability of different biomass. The inital thermal decompostion temperature for fructose, glucose, chitosan, and cellulose are 162, 197, 274 and 306 °C, respectively. The steady-state temperatures of the SPC process is about 260-270 °C.

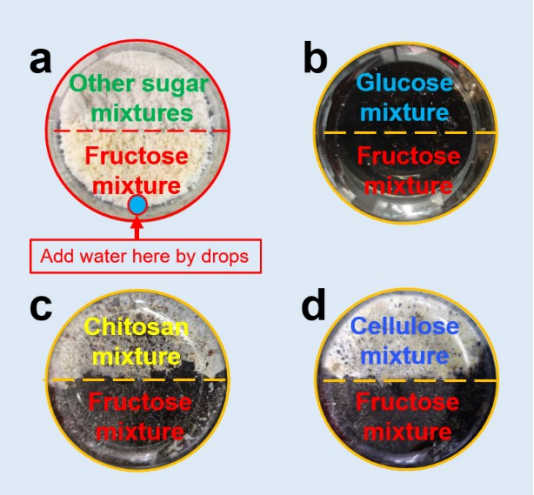

Figure S3. Use of fructose grinding mixtures to trigger the SPC process for other sugar mixtures.

We carried out an experiment as shown in Figure S3. The fructose mixture and the other sugar mixture were placed separately in a beaker and connected at the junction of the two (Figure S3a). Water was added to the fructose mixture from the end away from the dividing line to trigger the SPC process. The results showed that the glucose mixture bordering the fructose mixture was able to undergo SPC process induced by SPC process of fructose (Figure S3 b), while the chitosan and cellulose remained unreacted (Figure S3 c and d). This result confirms our hypothesis that the ability of the SPC process to proceed is related to the thermal decompostion temperature of the biomass.

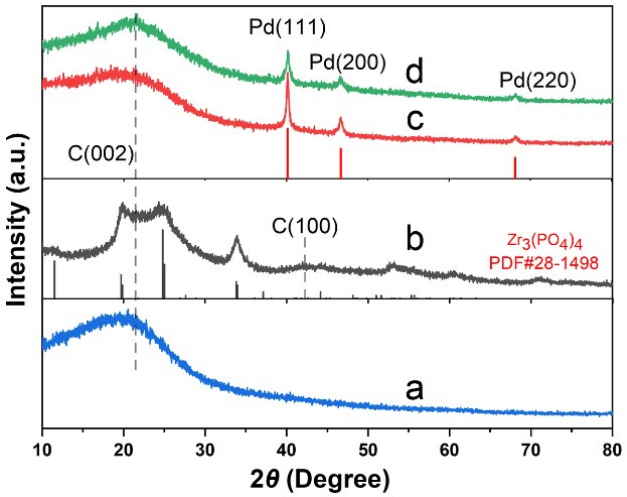

Figure S4. X-ray diffraction patterns of (a) PDC, (b) Zr/PDC, (c) Pd/PDC, and (d) PdZr/PDC.

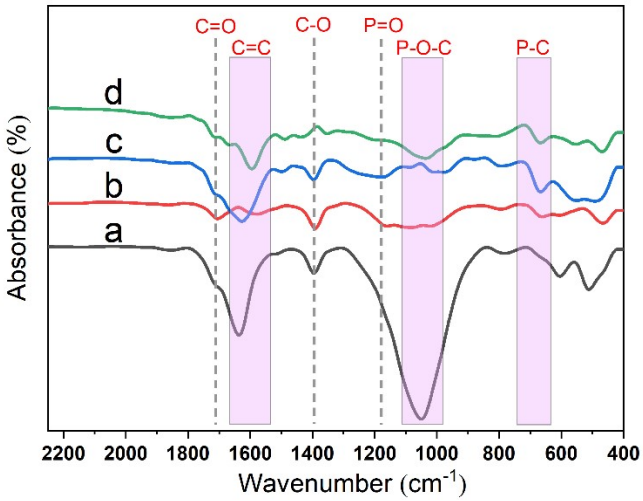

Figure S5. FT-IR spectra of (a) PDC, (b) Zr/PDC, (c) Pd/PDC, and (d) PdZr/PDC.

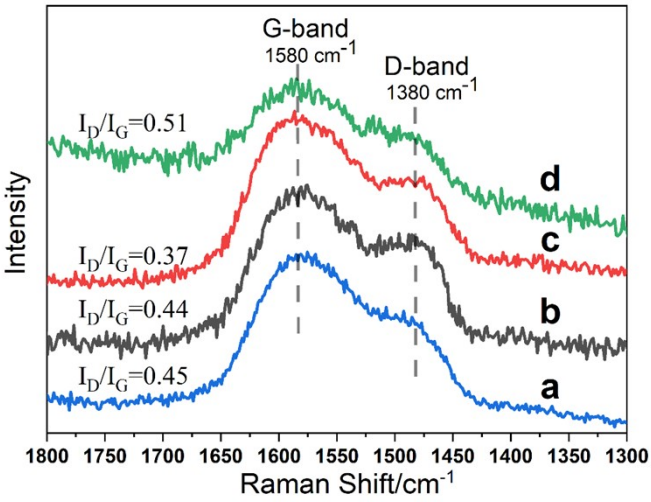

Figure S6. Raman spectra of (a) PDC, (b) Zr/PDC, (c) Pd/PDC, and (d) PdZr/PDC.

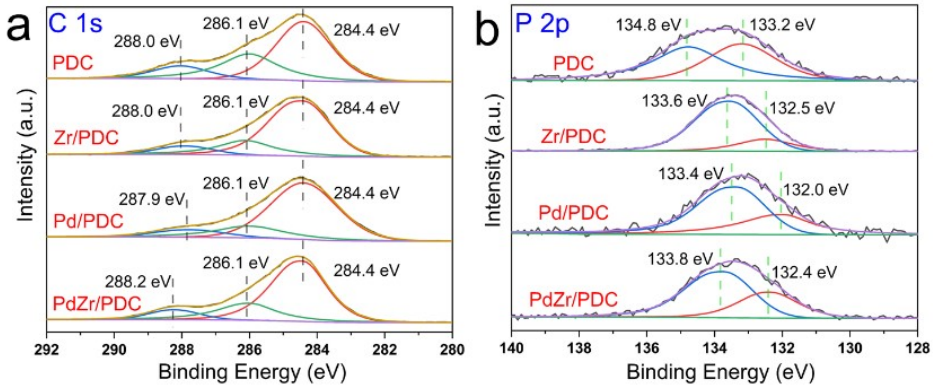

Figure S7. XPS spectra of (a) C1s and (b) P2p for PDC materials.

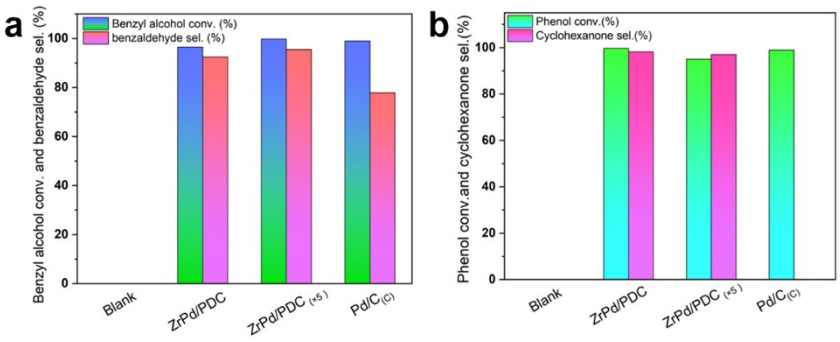

Figure S8. (a) Comparison of the catalytic oxidation performance of different catalysts; (b) Comparison of the catalytic oxygen hydrogenation performance of different catalysts.Reaction conditions for (a): 40 mg catalyst, 0.3 mmol benzyl alcohol, 3.0 mL (methanol : H_2O = 1:1), 60 ℃ (PdZr/$PDC_{(\times5)}$, 65 ℃), 3 h (PdZr/$PDC_{(\times5)}$, 4.5 h), 1000 rpm. ; reaction conditions for (b): 80 mg catalyst, 0.17 mmol phenol, 3.0 mL H_2O, 50 ℃, 6 h, 1000 rpm.

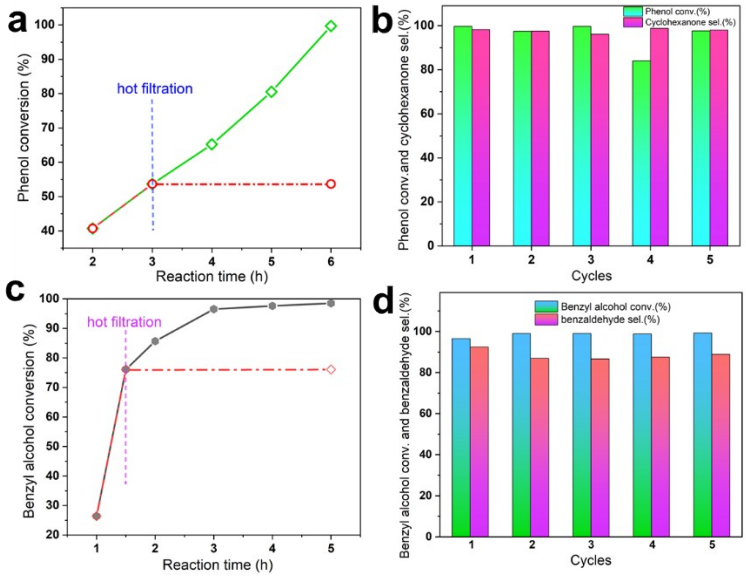

Figure S9. (a) Hot filtration experiment and (b) cyclic experiment of phenol hydrogenation conversion; (c) hot filtration experiment and (d) cyclic experiment of catalytic oxidation of benzyl alcohol. Reaction conditions for (a) and (b): 80 mg PdZr/PDC, 0.17 mmol phenol, 3.0 mL H_2O, 50 ℃, 6 h, 1000 rpm; reaction conditions for (c) and (d): 40 mg PdZr/PDC, 0.3 mmol benzyl alcohol, 3.0 mL (methanol : H_2O = 1:1), 60 ℃, 3 h, 1000 rpm.

Cyclic experiment: After the reaction, the catalyst was filtered out to test the recyclability. After washed alternately with methanol (3×5 mL) and water (3×5 mL), the catalyst was dried at 100 °C for 8 h. The used catalyst was directly applied in the next run under standard reaction conditions. In the hot filtration experiment, the catalyst was filtered when the reaction proceeded for a desired time, and the remaining solution continued to react under identical conditions. The reaction solution at the time of filtration and at the end of the reaction were respectively subjected to quantitative analysis to test the conversion of substrate and selectivity to product.

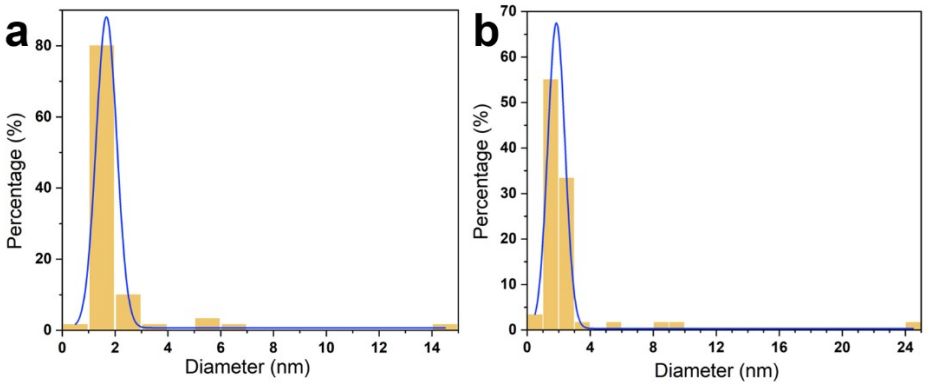

Figure S10. Particle size distribution of (a) Pd/PDC and (b) PdZr/PDC.

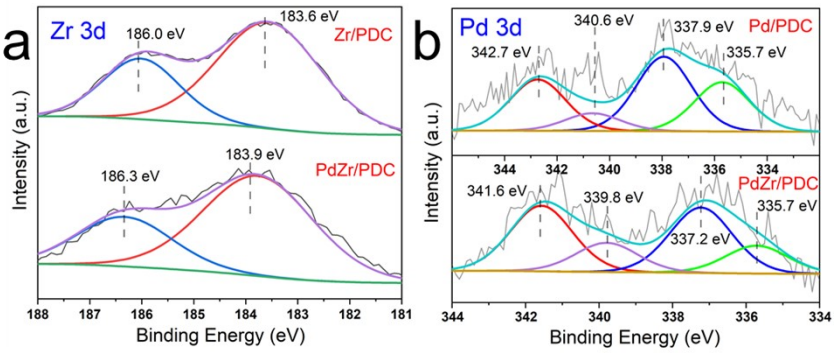

Figure S11. XPS spectra of (a) Zr 3d and (b) Pd 3d for PDC materials.

The XPS energy spectra show an increase in the binding energy of Zr to 186.3 eV and 183.9 eV in the PdZr/PDC sample compared to Zr $3d_{5/2}$ (186.0 eV) and Zr $3d_{3/2}$ (183.6 eV) in the Zr/PDC (Figure S11 a). indicating that there is electron transfer to the metal Pd. The Pd 3d XPS energy spectra in the Pd/PDC and PdZr/PDC samples are shown in Figure S b. The peaks at 335.7 and 340.6 eV in Pd/PDC represent the $3d_{5/2}$ and $3d_{3/2}$ orbitals of Pd^0, respectively, while the peaks at 337.9 and 342.7 eV represent the $3d_{5/2}$ and $3d_{3/2}$, respectively. This suggests an electronic interaction between the bimetals.

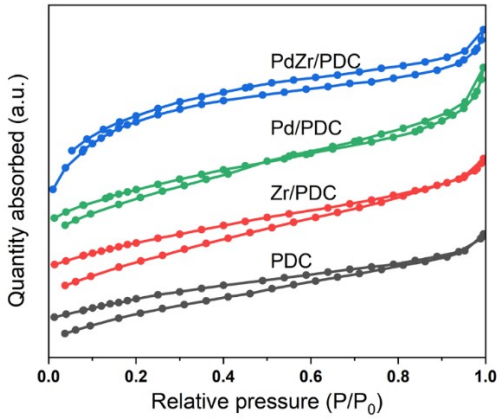

Figure S12. N_2 adsorption-desorption isotherms for the PDC series catalysts.

To understand the porosity characteristics of the PDC material, N_2 adsorption-desorption tests were carried out on the samples (Fig. S12). All PDC materials were found to exhibit similar isothermal profiles, showing sharp absorption at pressures of $P/P_0 < 0.1$ and slow absorption in the pressure range of $0.1 < P/P_0 < 0.9$, indicating the presence of microporous structures in the samples; at pressures of $P/P_0 > 0.9$, the isotherms of the PDC materials rose sharply, suggesting the presence of macroporous structures with microsphere accumulation in the materials.[17]

References

1. J. Xu, X.-T. Yi, T. Zhao, L.-Z. Wen, F. Wang and B. Xue, *Mol. Catal.*, 2021, **511**, 111749.
2. J. Yang, K. Cao, M. Gong, B. Shan and R. Chen, *J Catal.*, 2020, **386**, 60-69.
3. S. Tareq, Y. H. T. Yap, T. A. Saleh, A. H. Abdullah, U. Rashid and M. I. Saiman, *J. Mol. Liq.*, 2018, **271**, 885-891.
4. Y. Li, A. Chatterjee, L. B. Chen, F. L.-Y. Lam and X. Hu, *Mol. Catal.*, 2020, **488**, 110869.
5. N. M. JamJam, Y. H. Taufiq Yap, E. N. Muhamad, M. Izham Saiman and T. A. Saleh, *Inorg Chem Commun*, 2019, **107**, 107471.
6. J. X. Yaoqin Zhu, Ming Lu, *J. Iran. Chem. Soc.*, 2015, **12**, 1213-1219.
7. Q. Wu, L. Wang, B. Zhao, L. Huang, S. Yu and A. J. Ragauskas, *J. Colloid Interface Sci.*, 2022, **605**, 82-90.
8. C. Yang, K. Li, J. Wang and S. Zhou, *APPL CATAL A-GEN*, 2021, **610**, 117961.
9. C. Zhang, G. Yang, H. Jiang, Y. Liu, R. Chen and W. Xing, *Chin. J. Chem. Eng.*, 2020, **28**, 2600-2606.
10. G. Yang, J. Zhang, H. Jiang, Y. Liu and R. Chen, *APPL CATAL A-GEN*, 2019, **588**, 117306.
11. S. Xu, J. Du, Q. Zhou, H. Li, C. Wang and J. Tang, *J. Colloid Interface Sci.*, 2021, **604**, 876-884.
12. Y. Wang, J. Yao, H. Li, D. Su and M. Antonietti, *J. Am. Chem. Soc.*, 2011, **133**, 2362-2365.
13. P. Makowski, R. Demir Cakan, M. Antonietti, F. Goettmann and M.-M. Titirici, *ChemComm*, 2008, 999–1001.
14. H. Liu, T. Jiang, B. Han, S. Liang and Y. Zhou, *Science*, 2009, **326**, 1250-1252.
15. H. Liu, Y. Li, R. Luque and H. Jiang, *Adv. Synth. Catal.*, 2011, **353**, 3107-3113.
16. R. D. Patil and Y. Sasson, *APPL CATAL A-GEN*, 2015, **499**, 227-231.
17. J. Tang, M. Yang, F. Yu, X. Chen, L. Tan and G. Wang, *Appl. Energy*, 2017, **187**, 514-522.